Portable Droplet-based Real-time Monitoring of Pancreatic α-amylase in Postoperative Patients

Larysa Baraban (l.baraban@hzdr.de)
Helmholtz-Zentrum Dresden-Rossendorf https://orcid.org/0000-0003-1010-2791
Xinne Zhao
Helmholtz-Zentrum Dresden-Rossendorf
Fiona Kolbinger
TU Dresden https://orcid.org/0000-0003-2265-4809
Marius Distler
University Hospital Carl Gustav Carus, Technische Universität Dresden
Jürgen Weitz
Department of Gastrointestinal, Thoracic and Vascular Surgery, Medizinische Fakultät Carl Gustav Carus, Technische Universität Dresden, Dresden
Denys Makarov
Helmholtz-Zentrum Dresden-Rossendorf https://orcid.org/0000-0002-7177-4308
Michael Bachmann
Helmholtz-Zentrum Dresden-Rossendorf (HZDR)

Article

Keywords:

Posted Date: April 14th, 2023

DOI: https://doi.org/10.21203/rs.3.rs-2800086/v1

Additional Declarations: There is **NO** Competing Interest.

PORTABLE DROPLET-BASED REAL-TIME MONITORING OF PANCREATIC α-AMYLASE IN POSTOPERATIVE PATIENTS

Xinne Zhao[1,†], Fiona R. Kolbinger[2,3,†,*], Marius Distler[2], Jürgen Weitz[2,3], Denys Makarov[4], Michael Bachmann[1], Larysa Baraban[1,3,*]

[1] Institute of Radiopharmaceutical Cancer Research, Helmholtz-Zentrum Dresden-Rossendorf e. V., 01328 Dresden, Germany

[2] Department of Visceral, Thoracic and Vascular Surgery, University Hospital and Faculty of Medicine Carl Gustav Carus, TUD Dresden University of Technology, Germany

[3] Else Kröner Fresenius Center for Digital Health (EKFZ), TUD Dresden University of Technology, Germany

[4] Institute of Ion Beam Physics and Materials Research, Helmholtz-Zentrum Dresden-Rossendorf e. V., 01328 Dresden, Germany

† Contributed equally as co-first authors

* Corresponding authors:
Dr. Larysa Baraban, +49 (0) 351 2603091
e-mail: l.baraban@hzdr.de

Dr. Fiona Kolbinger, +49 (0) 351 458 19624
e-mail: fiona.kolbinger@uniklinikum-dresden.de

ABSTRACT

Postoperative complications after pancreatic surgery are frequent and life-threatening. Current clinical diagnostic strategies involve time-consuming quantification of α-amylase activity in abdominal drain fluid, which is taken on the first and third postoperative day. The lack of real-time data can delay adjustment of medical treatment upon complications and worsen prognosis for patients. We report a bedside portable droplet-based millifluidic device enabling real-time sensing of drain α-amylase activity for postoperative monitoring of patients undergoing pancreatic surgery. Here, a tiny amount of drain liquid of patient samples is continuously collected and co-encapsulated with a starch reagent in nanoliter-sized droplets to track the fluorescence intensity released upon reaction with α-amylase. Comparing the α-amylase levels of 32 patients, 97% of the results of the droplet-based millifluidic system matched the clinical data. Our method reduces the α-amylase assay time to approximately three minutes, which is a major improvement compared to the current clinical standard of several hours in the clinic. Furthermore, the device reveals an order of magnitude improvement in the limit of detection, reaching 7 nmol/s·L. The presented droplet-based diagnostics platform can be extended for analysis of different body fluids, diseases, and towards a broader range of biomarkers, including lipase, bilirubin, lactate, inflammation, or liquid biopsy markers, setting up new standards in clinical patient monitoring.

INTRODUCTION

According to the American College of Surgeons, every person may undergo up to 9 surgical procedures of different complexity per lifetime.[1] Global statistics show that approximately 300 million major surgeries are performed each year worldwide, with up to 4% resulting in death, 15% in serious postoperative morbidity, and 10-15% in readmission to the hospital within a few weeks.[2] This stimulates active development of new standards in patient care to mitigate post-operative complications. One way is increasing personalization of the post-operative monitoring, guided by novel diagnostic approaches.[3–6] As the detection of multiple critical biomarkers is still intermittent and lab-centralized, respective information about vital parameters and patient conditions comes with significant delays that critically affect the decision-making in post-operative therapy. Therefore, new technologies offering the ability of real-time and continuous monitoring of patients are urgently needed, ideally using portable equipment of bedside format.

Major abdominal surgeries are indispensable to cure benign and malignant diseases.[7] They are inevitably associated with postoperative complications that can be life-threatening. For pancreatic cancer, which is one of the most aggressive malignancies[8], curative treatment approaches obligatorily involve complete resection of the primary tumor through (partial) pancreatectomy. The most serious, yet a common complication after partial pancreatic resection is clinically relevant postoperative pancreatic fistula (CR-POPF), affecting up to 40% of patients.[9,10] It describes the leakage of pancreatic enzymes into the abdominal cavity, which significantly prolongs the inpatient stay and can frequently lead to delay or complete suspension of indicated adjuvant chemotherapy. This dramatically reduces survival of patients with pancreatic cancer.[11–13] In clinical practice, it is diagnosed by detecting elevated concentrations of the pancreatic enzyme amylase and lipase in the drainage secretions.[14–16] Currently, analysis of these enzymes is performed on the first and third postoperative day via collection of 1-5 ml of drain fluid (**Figure 1a**). Traditional laboratory chemistry methods for enzyme concentration measurement predominantly use colorimetric assays performed by laboratory personnel.[17] This approach, together with the typical clinical routine processes, *e.g.*, sample uptake, reagent preparation, measurements and communication, requires up to 6 hours to obtain results. Moreover, the method is not transferrable to bedside format due to multiple sample processing steps.

Thus, early determination of the enzyme concentration as well as its continuous monitoring in drainage secretions at the bedside is still missing and stimulates active ongoing explorations. There are reports on amylase sensors for the food and chemical industry,[18–22] biosensors for point of care diagnostics[23], *e.g.*, paper-based[24], or optical fiber biosensors.[25] Yet, none of these

technologies offer portable, real-time, and continuous monitoring of α-amylase in drain fluid in post-operative patients.

Droplet-based microfluidics that emerged a decade ago has offered a new route to manipulate fluids at femto- to nanoliter scale, which boosted efficiency of biochemical methods in terms of detection time and sensitivity.[26–30] Droplet-based fluidic platforms save reagent consumption and reduce experimental wastes, allowing for real-time and individual tracking of each reactor.[31] The technology has found numerous applications in biology and biotechnology.[18,32–39] Currently, this technology is applied for fundamental research[40], *i.e.,* food screening[41,42] and molecular sensing[43,44] and has proven useful for commercial applications, *e.g.*, PCR testing[45] **(Supplementary Table 1).**

To shorten the diagnostics time and to enable a reliable and real-time bedside check of the patient α-amylase in drainage secretions after abdominal surgery, we designed and clinically validated a portable droplet-based fluidics device. Our device can be conveniently placed at the patient's bedside (**Figure 1a**), collecting tiny amounts (max. 200 nL/s) of drain liquid hydrolyzed by mixing with a starch-FL reagent to generate fluorescent signals, for fully automated analysis of amylase concentrations. We collected samples from 32 patients and demonstrated that the α-amylase levels could be determined within 3 min at the precision level of 97% in agreement with the clinically standardized method. Our detection system outperforms the state-of-the-art clinical techniques by at least an order of magnitude in terms of limit of detection (LoD) and provides a 100-fold reduced detection time. The excellent LoD (7 nmol/s·L) allows using this device without further modifications in other body fluids and for other disease diagnostics *e.g.,* metabolic syndrome, diabetes (insulin insufficiency) and obesity[46,47], where the LoD in the range of 0.017-0.83 µmol/s·L is needed (**Supplementary Table 2**).[48–52] At the current operation rate, the minimum sample volume (drain liquid) required for a single measurement is approximately 10 µL (about 100 droplets for high statistical relevance). Even in the case of continuous α-amylase level monitoring of surgical patients, the maximum volume of drain liquid remains at the level of less than 20 mL per day which is within the same range taken for a single measurement in state-of-the-art clinical protocols. Therefore, in addition to the real-time tracking of the amylase level, further optimization of the enzyme monitoring strategy may lead to the significant saving of reagents and minimization of chemical wastes. The fluorescence intensity levels are calibrated against α-amylase concentration by measuring the reaction kinetics in the droplets passing the detector area. The demonstrated ability to precisely follow the changes in the α-amylase levels in the patient samples over time could markedly accelerate the diagnosis of the pancreatic leakage in general, beyond CR-POPF in early stages, which could improve recovery of patients after partial pancreatic

resection. We expect that this approach can be extended and transferred to other postoperative settings, including lipase, bilirubin, bacteria, or metabolites that, overall, would contribute to a rethinking of the technological standards in post-operative monitoring relying on high-throughput and high-precision fluidic technologies.

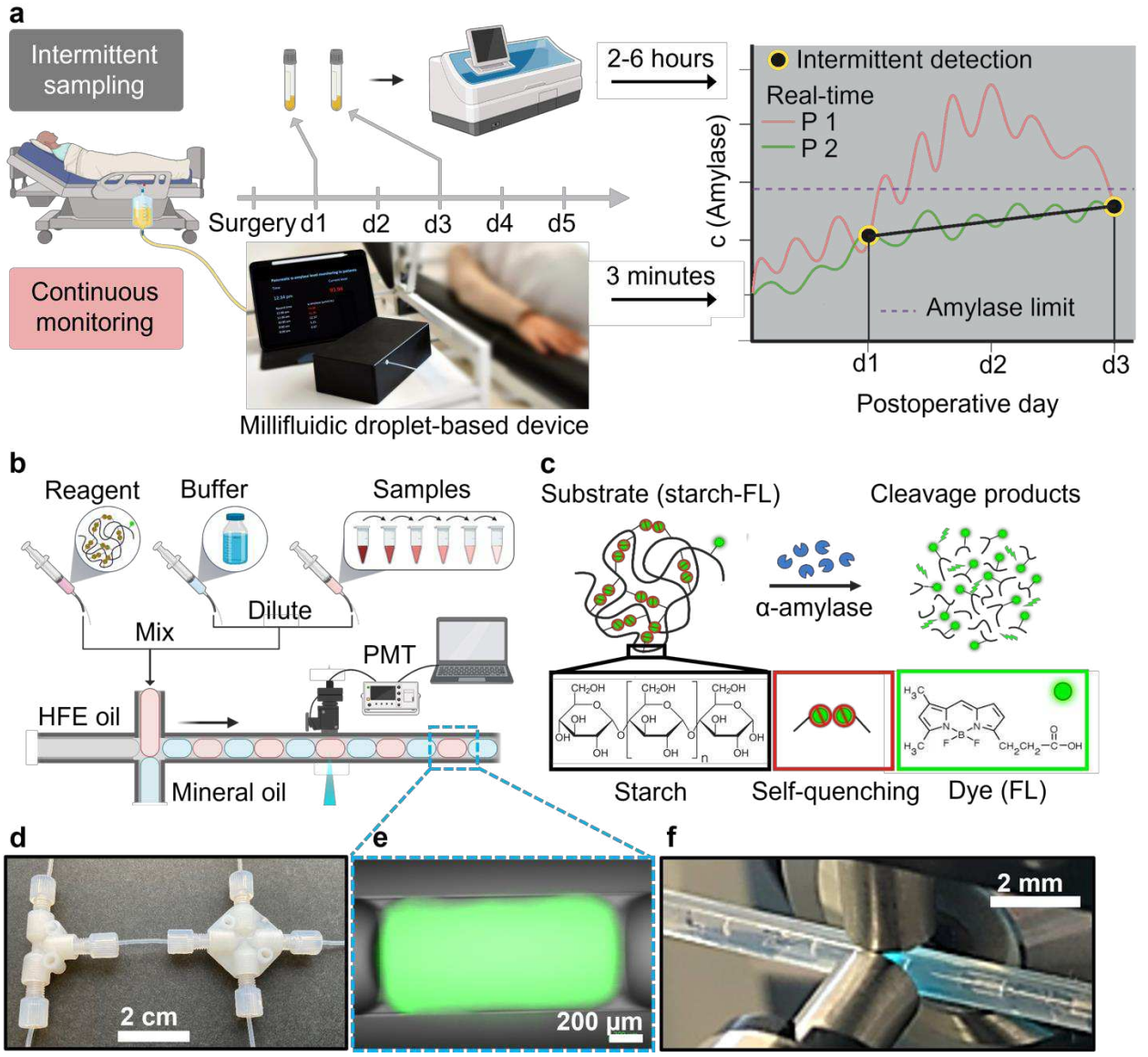

Figure 1: Concept illustration of abdominal drain α-amylase concentration detection using a droplet-based millifluidic device. **a.** Schematic comparison of α-amylase testing methods of clinical standard (standard intermittent detection performed at day 1 and day 3 after surgery) and the proposed droplet-based millifluidic device (real-time and continuous monitoring). After surgery, drainage secretions are passed from the surgical site in the abdomen to the outside via a drainage tube. In current clinical practice, the α-amylase concentration in drainage secretions is analyzed intermittently on the first and third postoperative days (duration of sample processing and analysis in clinical practice: 2-6 hours). In contrast, the proposed droplet-based millifluidic device could be conveniently placed at the patient's bedside and continuously monitor α-amylase concentrations in near real-time (red and green curves mimic the possible amylase real-time evolution from the

drained liquid of patient P1 and patient P2). **b.** Schematic illustration of α-amylase detection in droplet-based millifluidic reactors. Reagent, buffer, and pre-diluted drainage secretion samples are injected into the tubing and meet at T- and cross-junctions **d** to form droplets. **c.** Schematic illustration of α-amylase reaction with the substrate reagent (corn starch conjugated with a fluorescent dye, starch-FL), resulting in cleavage products emitting fluorescence proportional to the α-amylase concentration. **e**. The fluorescence micrograph of an aqueous droplet (200 nL) with the green fluorescence resulting from the reaction in panel c. **f.** Patient samples react with the starch-FL reagent and emit fluorescence in the droplets-based reactors, passing through the illumination and photomultiplier tube (PMT) detector.

RESULTS AND DISCUSSION

α-*Amylase calibration using droplets analyser*

The droplet-based millifluidic device (**Figure 1b, d-f**) for α-amylase detection consists of droplet generation and detection areas (**Supplementary Figure 1**). In the generation area (**Figure 1b**), 200 nL droplets are formed by injecting the aqueous phase (contains starch-FL reagent, reaction buffer, and α-amylase; pink color), mineral oil (spacers, blue color) and hydrofluoroether (HFE) oil (with 1% surfactant PicoSurf 2^{TM}, gray color) to the cross-junction (**Figure 1d**) using a pump (Nemesys, Cetoni). A chain of droplets (**Figure 1e**) is injected into the capillary tubing and pushed toward the photomultiplier tube (PMT) detector (**Figure 1f**), where the fluorescence emitted from the droplets is detected and recorded using LabView.[53]

The detection of the α-amylase concentration builds upon the reaction between the starch-FL reagent (corn starch conjugated with a fluorescence dye, starch-FL, intramolecular self-quenching) and α-amylase, which produces cleavage products (self-quenching disruption), resulting in the enhancement of the fluorescence intensity that is emitted by the droplets (**Figure 1c**). In this respect, the droplet format is superior to continuous flow options, *e.g.,* lateral flow devices, *etc*., due to the close localization of the reagents and fluorescent reaction products within a small volume that shortens a time to the detection. For calibration purposes, we detect 600 droplets within one assay and average detected enzymatic activity to determine the α-amylase concentration. Droplets are detected at a frequency of 2.2 droplets per second to record the fluorescence signal generated by the reaction between α-amylase and starch-FL reagent. In this experiment, we fixed single reactor volume as 200 nL, which is 500 times smaller than a single microplate well (100 µL). Due to this small volume of the millifluidic droplets the detection time is shortened (**Supplementary Figure 2b** in droplets *vs* **Supplementary Figure 3a** in microplates), and a lower reagent amount (10% of the samples, reagents, and buffers, compared to microplate method) is used to record the reaction process. Thus, this format has a potential to significantly reduce the consumption of chemicals, as shown in **Supplementary Table 3**, and to minimize chemical waste.

For validation of the method, calibration measurements were first performed using standard samples to relate the different α-amylase concentrations to the fluorescent signal, as described in **Supplementary Figure 2**.

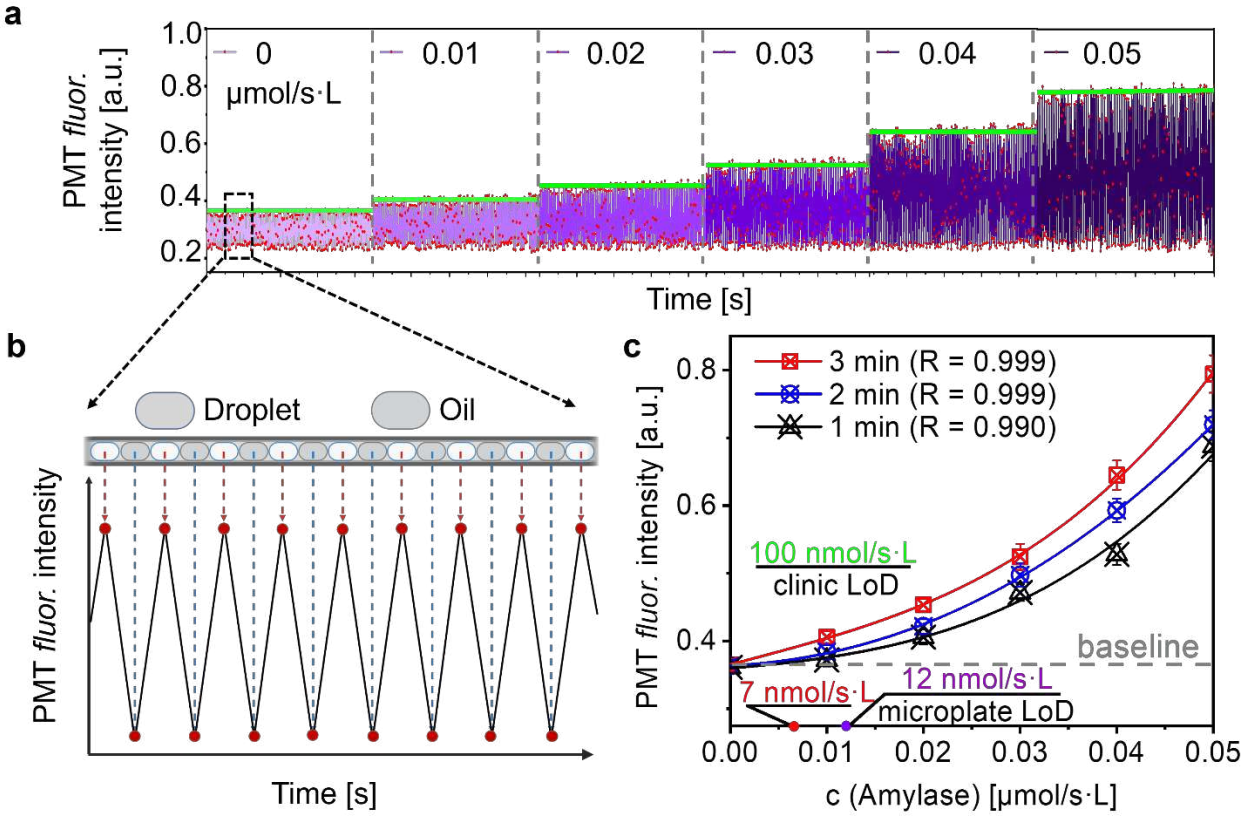

Figure 2: Calibration curve of α-amylase concentration and fluorescence intensity for the droplet-based millifluidic system. a. Concentration-dependent changes in fluorescence intensity based on the reaction between the reagent and standard α-amylase solution (with various concentrations) in droplet-based millifluidic reactors. **b.** Close-up view of the droplet sequence and its corresponding fluorescence signal. The peaks result from droplets (white), and the valleys represent the mineral oil (gray). The fluorescence intensity of the droplet was obtained by averaging the fluorescence intensity (green lines in panel A) of 100 peaks (droplets) after 3 min reaction. **c.** A plot of fluorescence intensity and related α-amylase concentrations and corresponding fit curves after 1-, 2-, and 3-min. Abbreviations: a.u.: arbitrary units, *fluor.:* Fluorescence, LoD: limit of detection, PMT: Photomultiplier tube.

Droplets with higher injected α-amylase concentrations (up to 50 nmol/s·L) emitted a higher level of fluorescence intensity of the α-amylase-starch reaction (**Figure 2a** and **Supplementary Figure 2**). The peaks generated by 100 droplets were averaged (green line) to obtain the fluorescence intensity at the selected reaction time point (**Figure 2b**). The averaged values were further plotted against the corresponding α-amylase concentration to obtain the calibration curves at different reaction time points (**Figure 2c,** and **equation (1)** in ***Materials and Methods***). Important to note, the efficient detection of the amylase in droplets can be achieved already at 60 seconds (see black

line in **Figure 2c**), which is much faster than offered by other reported methods, and in particular current clinical standard methods, which require about 2-6 h. Based on the fitted curves, the LoD at the given values of the amplification of the PMT (see **equations (2, 3)** in ***Materials and Methods***) was calculated to be 7 nmol/s·L.[54] The same calibration procedure was performed using the standard technique in the clinic (UV-Vis spectrometry) resulting in LoDs of 100 nmol/s·L. Therefore, the droplet-based millifluidic system revealed a much lower LoD (7 nmol/s·L) and shorter time (60 seconds) for α-amylase measurement compared to all reported methods (see comparison in **Supplementary Table 3**). Fluorometry in microplates was used as a reference technique in these experiments (see ***Materials and Methods*** and **Supplementary Figure 3**).

α-Amylase detection in patient samples

To measure α-amylase concentrations in patient samples, we fix the time between mixing the reagents in droplets and detection event to 3 min, which corresponds to the calibration curve in **Figure 2c** (red line). For the following analysis the collected drain liquid was injected into droplets containing the starch-FL reagent (0.02 mg/mL). The fluorescent signal emitted from each droplet reactor was detected by the PMT and constantly recorded by the self-developed LabView software (**Figure 3a**). For instance, exemplary patient samples #2, #8, #15, and #28 (see all patient sample results in **Supplementary Figure 4**) showed various amylase concentrations upon using calibration curve and considering the dilution factor (see dilution factor determination and details in ***Materials and Methods***), α-amylase concentrations of patient samples were obtained (sample #2: 553.30 µmol/s·L; sample #8: 0.013 µmol/s·L; sample #15 3.47: µmol/s·L; sample #28: 122.76 µmol/s·L).

To demonstrate the stability and reproducibility of the droplet-based millifluidic method, we measured samples repetitively 3 times (**Figure 3b, c**). Samples were frozen and stored after the first measurement to keep the composition stable. The replicated results proved that the millifluidic method offers great stability in testing the identical samples, as well as the microplate methods (**Supplementary Figure 5**).

In parallel to the droplets format (duration 3 min, 100 droplets, sample drain volume 10 µL, reagent volume 10 µL (starch at concentration of 0.02 mg/ml), each patient sample was also analyzed in clinic using UV-Vis spectrometry in colorimetric format (duration up to 6 h, samples volume 1-5 mL, reagent volume 1-5 mL in two step reaction). As control, we also performed fluorescence analysis of samples measured in microtitre plates (Cytation 5, samples volume 300 µL, reagent volume 300 µL (0.2 mg/mL)). By comparing the α-amylase concentrations detected by three different methods, we found a very good matching of the results from all 32 patient samples. In

particular, following panels **d** and **e** in **Figure 3** summarize the comparative analysis between the droplet-based millifluidics and clinical standard clinical UV-Vis method. Further studies, *i.e.,* comparison to the reference fluorescent microplate is summarized in **Supplementary Figure 6a, b**).

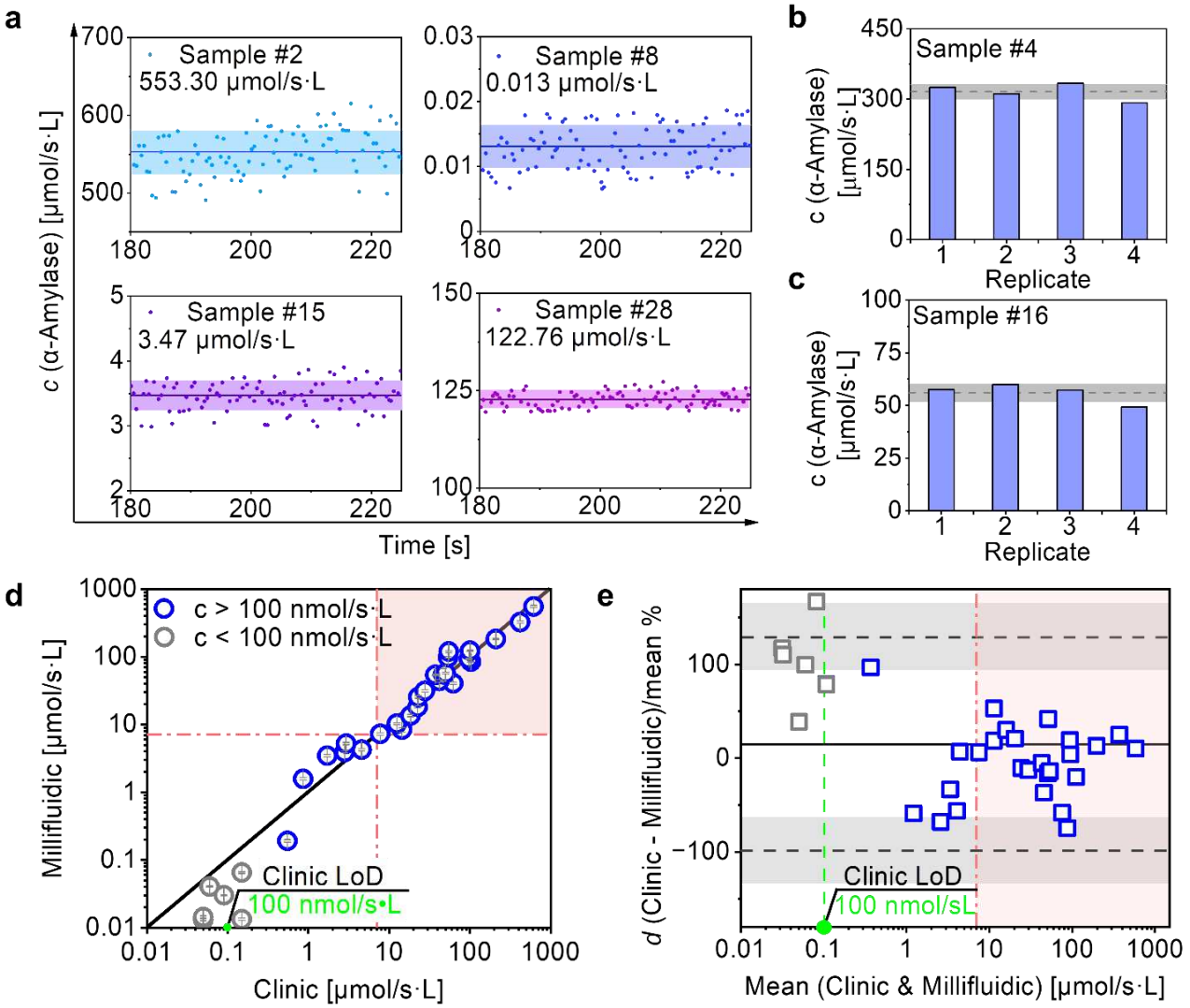

Figure 3: Detection of α-amylase concentrations in patient samples using the droplet-based millifluidic system. Correlation and Bland-Altman agreement analysis of the results between the clinical standard and droplet-based millifluidic methods. **a.** α-Amylase concentration of arbitrarily selected samples #2, #8, #15, and #28 (see all 32 patient sample results in Supplementary Figure 4 and Supplementary Table 4). The solid line is the average concentration, and the colored area is the error bar (standard deviation). α-Amylase concentration tested in 4 replicates of the sample #4 (**b.**) and sample #16 (**c.**). **d.** Correlation of α-amylase detection results between the clinic and millifluidic methods. The solid black line represents y = x. The x-axis and y-axis are represented in $\log_{10}$. **e.** Bland-Altman agreement plot of results from the clinic and millifluidic methods. The x-axis displays the mean value measured by two methods (in $\log_{10}$ scale); the y-axis represents the ratio of the difference between the measured values of the two methods to the mean value. The black line represents the mean of the difference ($\bar{d}$, black dash lines). The limits of agreement in 95% confidence are from -1.96σ to +1.96σ (σ, standard deviation) with

confidence intervals (gray areas). The pink dashed lines in (d) and (e) represent the upper limit of the normal range of drain amylase, defined as an amylase level >3 times the upper limit of institutional normal serum amylase activity, *i.e.,* 7 µmol/s·L.[55]

Namely, Pearson correlation (**Figure 3d**) and Bland-Altman agreement studies (**Figure 3e**) were performed to quantitatively compare the droplet-based method to the clinical standard. Note, while the comparison is done for all patients' data, a mismatch in the LoDs of both methods (7 nmol/s·L vs. 100 nmol/s·L) does not allow a proper correlation of the results at the concentrations below 100 nmol/s·L (grey data points in **Figure 3d and Figure 3e**). Therefore, the discussion below is dedicated solely to the 26 patient samples (blue data points) with amylase concentration higher than the LoD of the clinical method. Pink colored areas in (d) and (e) correspond to the range of concern for the elevated α-amylase concentrations, defined as 3 times the upper limit of institutional normal serum amylase activity, *i.e.,* 7 µmol/s·L.[55] For the droplet-based millifluidic method, the coefficient of determination (R^2 = 0.97 and Pearson's correlation coefficient (r = 0.95) proved that the results of the clinical and millifluidic methods have a great linear correlation in the clinically relevant dynamic range of the measurements,[56,57] (see **Supplementary Figure 6a, b**). Compared to the clinic method, the correlation between microplate and millifuidic methods (**Supplementary Figure 6c**) appears to be much better because of the better matching of the LoDs of these two techniques (c of about 100 nmol/s·L and below).

Also, a Bland-Altman analysis[58,59] demonstrated the quantitative agreement between two methods (see details in ***Methods***) (**Figure 3e**). Overall, 31 out of 32 (97%) samples measured with the millifluidic method matched excellently with clinical measurements within the 95% confidence interval, and 100% (26/26) of paired values lie inside the limits of agreement in the concentration range where clinical method is accurate, c > 100 nmol/s·L (**Figure 3e** and **Supplementary Table 5**). Moreover, for the Bland-Altman analysis between different methods (**Supplementary Figure 7a, b** and **Supplementary Table 6, 7**)**,** we noticed the bias in paired data is relatively greater at low concentrations. This, on the one hand, is due to the mismatched LoDs; on the other hand, may be caused by sample conditions, *e.g.,* pH value and viscosity of original samples without dilution that might have affected the reaction sensitivity and kinetics. Diluting the sample helped to alleviate this problem. Unlike the standard α-amylase solutions used for calibrations, the viscosity of the patient sample does vary due to impurities such as blood cells, cellular detritus, or tissue fluid. This could lead to slightly different sensitivities and speeds in the reaction with the reagent.

Continuous monitoring of amylase concentrations using droplet-based millifluidics

Since the droplet system was demonstrated to be capable of accurate and fast determination of the α-amylase concentration in drain liquid from patients, we next explored the option of continuous monitoring of the enzyme level in the ascites drainage. Given the exploratory character of the study, direct monitoring of patients was not yet possible. Therefore, we simulated possible fluctuations of α-amylase concentration in patient samples via preprogrammed dilution of the clinical sample over time. We recorded the change in fluorescence intensity in approximately 5300 droplets over 40 min (**Figure 4)** and correlated it with the calibration curve (**Figure 2c**) to get the instantaneous value of the α-amylase level in the sample.

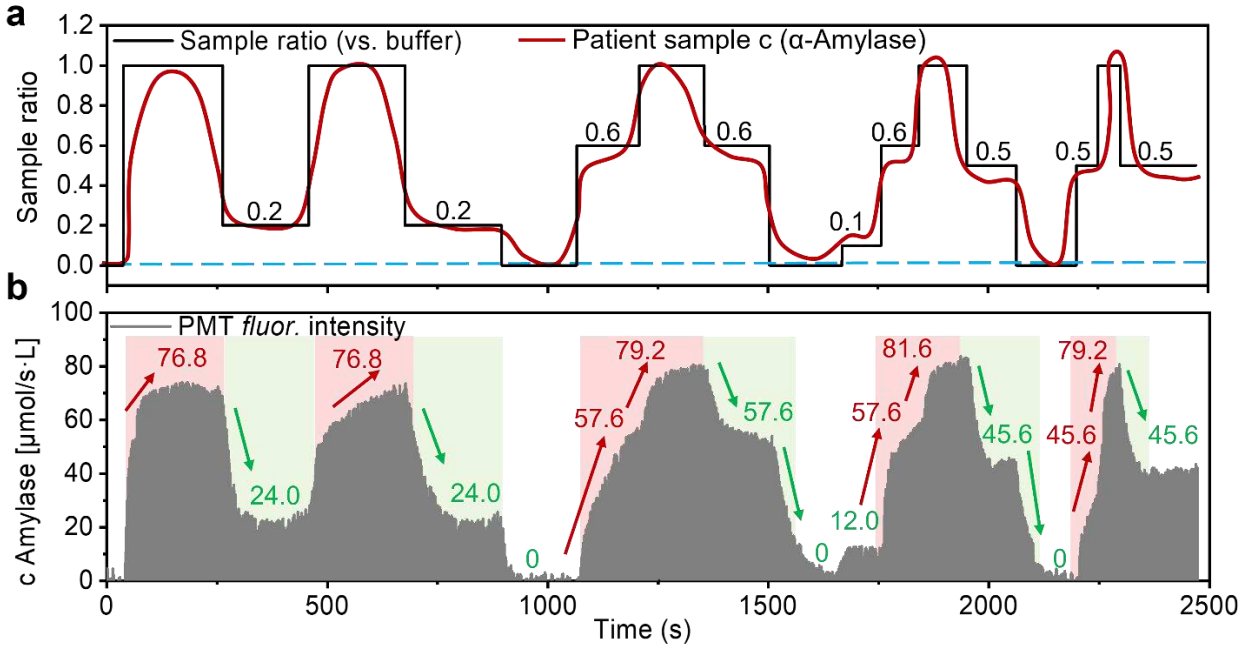

Figure 4: Continuous detection of patient sample α-amylase concentrations in the droplet-based millifluidic system. a. Schematic of pre-set changes in α-amylase concentrations of patient samples (red) over time and the simulation of the α-amylase concentration (patient sample) fluctuations with the droplet-based millifluidic system (black). Sample #26 was arbitrarily chosen for this experiment. Sample Ratio '1' was the droplets containing 100% sample, and '0' meant the droplets contained 100% buffer (baseline). **b.** Amylase concentration (related fluorescence intensity) of the droplet sequence with the corresponding α-amylase concentration fluctuations was measured with the millifludic system. The red and green areas with ascending or descending arrows indicate the different stages of α-amylase concentration change.

To create and mimic the arbitrary fluctuations of the α-amylase level (as demonstrated by, *e.g.,* red line, **Figure 4a**), the ratio between the buffer and patient sample (Sample #26) was programmed to tune during the generation of the droplets ('1' - 100% sample and '0' - 100% buffer), as shown in **Figure 4a** (black). During the continuous passage of the droplet sequence through the PMT detector, we recorded the changes in fluorescence intensity and related them to the sample concentrations (**Figure 4b, c**). Overall, the amylase concentration measured by

fluorescence signal changes accurately reflected the dilution profile of the patient sample shown in panel A (black) and mirrored the changes in α-amylase concentration. Notably, the amylase concentration (related fluorescence signal) always reached similar levels at identical sample ratios. It precisely coincided with the preprogrammed manipulation of the dilution factor, indicating that the system could capture fluctuation of α-amylase concentration in real-time and perform continuous detection without limitations regarding detection duration and the number of droplets. This proof-of-concept demonstration gives great promise that the droplets-based system might be involved in the real-time monitoring of patients in future clinical practice. Therefore, for long-term measurements, further developments of the setup are to be done, for instance, to consider the effects of the inertia of the fluidic circuit and patient sample variability, *e.g.,* different viscosities and pH values.

CONCLUSION

This study reports a method for near-real-time detection of absolute value of drain fluidic pancreatic α-amylase in a droplet-based millifluidic system, facilitating automatic continuous and personalized diagnostics at the bedside. The droplet-based fluidic format offers portability and shortens the detection time to a minute, compared to several hours of the current technique applied in clinical practice. Furthermore, this experimental method offers improvement of the limit of detection to 7 nmol/s·L, which is about 14 times lower compared to the clinical counterpart. Our method requires ca. 10 µL of drain liquid (*vs.* 1-5 ml in clinics) for successful and precise detection. Correlation and agreement analysis showed that 31 out of 32 (97%) samples measured with the millifluidic method matched excellently with clinical measurements within the 95% confidence interval (and 100% (26 out of 26) match in the concentration ranges, where both methods are comparable, $c > 100$ nmol/s·L). By simulating fluctuations in α-amylase concentration, we demonstrate the rapid response of fluorescence intensity to sample concentration fluctuations in the millifluidic system, suggesting that the method can be implemented to continuously monitor drain α-amylase concentrations after pancreatic surgery. Overall, the presented results suggest that the proposed droplet-based device for detecting α-amylase activity in drain fluid of patients delivers the results with high precision, great stability and reproducibility, a faster detection time and lower LoD when compared to the standard clinical method. The proposed method is capable of monitoring clinically relevant changes (*i.e.* rapid increases) in drain α-amylase levels. It has the possibility to use such an instrument in real clinical settings for, *e.g.,* highly sensitive and stable monitoring of pancreatic enzyme activity over time using the droplet-based millifluidic system.

Thus, we are confident that this technology could markedly accelerate the diagnosis of pancreatic leaks in its early stages and improve the recovery of patients after partial pancreatic resection in the short, medium, and long term. While the level of concern for the amylase in drain liquids is only around 7 µmol/s·L and may reach up to 600 µmol/s·L, our method adequately covers the whole critical dynamic range necessary for the diagnostics of the patients after pancreatic surgery. Substantial backup in the dynamic detection range, achieved thanks to the low LoD of the droplet-based millifluidic device (7 nmol/s·L), paves the way for exploring the precise amylase sensing in the other body fluids (*e.g.*, blood, urine) with the typically lower ranges of the analyte concentrations (**Supplementary Table 2**). This is of crucial importance for the diagnosis of other related diseases, *e.g.,* metabolic syndrome, diabetes (insulin insufficiency) and obesity.

Overall, all aforementioned qualities of the device are exactly the key enablers for the novel format of the postoperative monitoring of patients at the bedside. Therefore, we are sure that this concept could be transferred to further relevant analytes such as, bilirubin or inflammation markers, thereby setting new standards of diagnostics, monitoring, and surgical intensive care. Note the time-dependent correlation of various markers measured in parallel could enable a more precise determination of the patients' health status in the future. Technically, this should be realized via multiplexing of fluorescent measurements and the simultaneous establishment of several assays within every single droplet.

Ultimately, the utility of the instrument has the potential to be extended towards a broader range of diseases and complications, as well as testing patient response to the therapy. Here, analysis of the diverse species, *e.g.*, lactate, lipase, creatinine, *etc.*, in different body fluids, *e.g.,* drain, blood, and interstitial fluid, are the logical next applications of the device due to the ability to explore the enzymatic nature of the reactions. Moreover, other markers relevant to liquid biopsy and involving new diagnostic approaches, *e.g.,* CRISPR-based methods, can be explored.

MATERIALS AND METHODS

Patient samples

Between March 2022 and June 2022, a total of 32 drain fluid samples (2 x 9 mL) from patients having undergone partial pancreatic resections (pylorus-preserving pancreaticoduodenectomy, Whipple’s procedure or distal pancreatectomy) at the University Hospital Carl Gustav Carus Dresden, Germany, were gathered in serum tubes (#02.1063.014, Sarstedt, Nümbrecht, Germany). α-Amylase concentration in one sample of each pair was analyzed at the Institute for

Clinical Chemistry and Laboratory Medicine at the University Hospital Carl Gustav Carus Dresden, Germany, using a colorimetric assay (#05167035, Roche, Basel, Switzerland) and a Cobas® 8000 high-throughput modular analyzer (Roche, Basel, Switzerland) as the standard method. In parallel, the other sample was analyzed using microplate measurements and droplet-based millifluidics.

All included patients had a clinical indication for the surgical procedure. This study was performed in accordance with the ethical standards of the Helsinki declaration and its later amendments. The local Institutional Review Board (ethics committee at the Technical University Dresden) reviewed and approved this study (approval number: BO-EK-76032013). Written informed consent was obtained from all patients. All patient samples were stored at -20° C for up to 14 days before measurement. Before measurement, the samples were de-frozen and centrifuged to collect the supernatants and pre-diluted. Pre-dilution allows the reduction of a highly concentrated sample to be within the calibration curve range for α-amylase. Furthermore, dilution results in adjusting the pH value and a decrease in viscosity, and reduction of inhomogeneity of the samples. This enables reduction of viscosity-related variability in reaction speed with the reagent.

Solutions Preparation

To detect α-amylase concentrations, the fluorometric α-amylase assay kit (EnzChek™ Ultra, Thermo Fisher) was chosen as the reagent and α-amylase (from Bacillus sp., Merck) as standard α-amylase samples. In the kit, the reagent (BODIPY®@FL-DQ™) is starch from corn that is conjugated with a fluorescence dye (starch-FL, intramolecular self-quenching). Once the reagent reacts with α-amylase, the cleavage products (self-quenching disruption) of the reagent show high fluorescence, as demonstrated in **Figure 1b**.[60] The original reagent solution (1 mg/mL) was prepared by dissolving 1 mg starch-FL reagent into 100 µL reagent solvent (50 mM sodium acetate, pH 4.0) and 900 µL 1 × reaction buffer (diluted from 10 × reaction buffer, 0.5 M MOPS, pH 6.9). This prepared reagent solution can be efficiently broken down by α-amylase and releases a strong fluorescence proportional to the α-amylase activity. First, 100 mg α-amylase was dissolved in 22.56 mL reaction buffer to obtain the original standard stock α-amylase solution with concentration of 1.0×10^7 U/L (1.67×10^5 µmol/s·L). The original stock α-amylase solution was then diluted to different concentrations as the standard α-amylase solutions required.

Microplate Fluorometry

Calibration curve: To establish an α-amylase concentration to the fluorescence intensity calibration curve (**Supplementary Figure 3**), a set of standard α-amylase solutions (with

concentrations of 8.33 µmol/s·L, 2.5 µmol/s·L, 0.83 µmol/s·L, 25 µmol/s·L, 0.25 µmol/s·L , 0.17 µmol/s·L, 0.083 µmol/s·L, 0.042 µmol/s·L, 0.017 µmol/s·L, and blank 0 µmol/s·L) was prepared by diluting the original solution (1.67×10^5 µmol/s·L) with the reaction buffer (0.05 M MOPS, pH = 6.9). Then, 50 µL of each dilution was pipetted to black 96-well plates (triplicates), followed by adding 50 µL reagent reaction solution (0.2 mg/mL, 200 µL original reagent solution diluted with 800 µL buffer and mixed well) to each well. The well plates were quickly transferred to the plate reader (Cytation 5) and measured at an excitation wavelength of (485 ± 12) nm and an emission wavelength of (520 ± 12) nm. Measurements were taken at room temperature every 5 min until 60 min. The plate was shaken before each data collection.

Based on the tracked change in the fluorescence intensity caused by the reaction between α-amylase (standard solutions of different concentrations) and identical amounts of the starch-FL reagent, higher α-amylase concentrations led to a faster increase in fluorescence intensity, reaching saturation more quickly, as shown in **Supplementary Figure 3a**. The fluorescence intensity showed a linear relationship with α-amylase concentrations between 0 and 0.83 µmol/s·L over a reaction time of 20 min, as shown in **Supplementary Figure 3b**. According to the calibration curve of fluorescence intensity to the α-amylase concentration (insert graph), the LoD was calculated to be 12 nmol/s·L (see **equation (2)** and **equation (3)**), lower than the LoD of the clinical standard method of 100 nmol/s·L.

The equation of linear fitted calibration curve of the microplate method (**Supplementary Figure 3b**): fluorescence intensity = 0.222 + 7.295 *c*,

where *c* is the concentration of amylase (µmol/s·L).

Patient sample measurement in microplates: The frozen patient drain fluid samples were first de-frozen and centrifuged (miniSpin plus, Eppendorf) at 6700 rpm for 10 min to collect the supernatant. The supernatant was diluted from 1 to 2^{15} in triplicate. Of each dilution (triplicates), 50 µL was added to the black 96-well plates, adding 50 µL reagent reaction solution (0.2 mg/mL) to each well. Samples in well plates were measured following the same protocol outlined above for the standard solutions.

Droplet-based millifluidics

Due to the small volume of the droplet-based millifluidic reactor (200 nL), the concentration of the reagent solution used in the droplet-based millifluidic system was 0.02 mg/mL (10% of the one used for experiments in microplate). The standard α-amylase solutions, the reagent solution (0.02 mg/mL) and the reaction buffer (0.05 M MOPS, pH = 6.9) were filled in glass syringes (SGE 2.5 mL and SGE 5 mL) and subsequently pumped into the fluidic system in FEP (fluorinated ethylene propylene) tubing (**Figure 1 d-f**). The reagent solution and the buffer met at a T-junction

(ethylentetrafluorethylen, ETFE) to form the aqueous phase with a total flow rate of 5 mL/h. In the aqueous phase, the reagent flow rate was constant at 2.5 mL/h, and the α-amylase solution and reaction buffer were 2.5 mL/h in total. The mineral oil (Sigma-Aldrich) worked as blockers, and HFE oil (hydrofluoether, Novec 7500, IoLiTec Ionic Liquids Technologies GmbH) mixed with 1% surfactant (PicoSurf 2^{TM}, Dolomite Center Ltd.) worked as the continuous oil phase. The aqueous phase, mineral oil, and HFE oil were pumped into the fluidic system with a flow rate ratio of 5:5:1 mL/h and met at the cross-junction (ETFE) to generate aqueous droplets separated by HFE oil. Droplets were then transferred to the detection area, where the fluorescence detector PMT (photomultiplier tube, HAMAMA) was used to collect the fluorescence signal from droplets. An illumination (488 nm, Thorlabs) with an optical lens (482 ± 9 nm, Thorlabs) was used to excite the samples. An optical emission filter (520 ± 14 nm, Thorlabs) and an optical objective (10×, Zeiss) were used to filter and focus the fluorescent light into PMT. The collected fluorescence signal by PMT was recorded by a laptop, as shown in **Figure 1b**.

Calibration curve: Five droplet sequences were generated. In each of the sequences, the concentration of α-amylase standard solutions in the aqueous droplet changed from 0 μmol/s·L to 0.05 μmol/s·L in 0.01 μmol/s·L intervals in different sequences, and the reagent was kept constant in each droplet. Each droplet sequence containing around 600 droplets passed through the detector PMT with a flow rate of 5 mL/h to record the fluorescence intensity. The droplet sequences with different concentrations showed different fluorescence intensities, as shown in **Figure 2a** and **Supplementary Figure 2**. In the plot, each peak of the data point represented an aqueous droplet. Each valley of the data point was a mineral oil drop (**Figure 2b**). The calibration curve was plotted by taking the data at 180 s (3 min) for each droplet sequence (average fluorescence intensity from 100 droplet peaks), as shown in **Figure 2c**.

The equation of polynomially fitted calibration curve (**Figure 2c**) of the droplet-based millifluidic method:

$$PMT\ Fluorescence\ intensity = 0.365 + 0.064c - 0.003c^2 + 0.010c^3 \quad (1)$$

where *c* is the concentration of amylase (μmol/s·L).

Patient samples measurement: The frozen samples were first de-frozen and centrifuged (miniSpin plus, Eppendorf) at the speed of 6700 rpm for 10 min. Then the supernatants were collected and filled into syringes. In the same condition as the standard α-amylase solutions detection described above, the patient samples were mixed with a certain amount of reagent and buffer and pumped to pass through the detector. The degree of dilution was adjusted to fit the intensity of the fluorescence signal to the detection range of the PMT. The fluorescence intensity of each sample was obtained by averaging 100 droplet peaks. The various amylase concentrations of 32 samples

were obtained upon using calibration curve and considering the dilution factor, as shown in the equation:

$$c(Amylase)_{patientsample} = dilutionfactor \times c(Amylase)_{millifluidic}$$

For instance, in **Figure 3a**, Sample #2 has a dilution factor of 1.5 × 10^4 and PMT fluorescence intensity correlated amylase concentration of 0.0369 μmol/s·L, so the calculated α-amylase concentration of 553.30 μmol/s·L. Sample #8 has a dilution factor of 1 and the calculated concentration of 0.013 μmol/s·L ($c(Amylase)_{millifluidic}$ = 0.0133 μmol/s·L). Sample #15 has a dilution factor of 100 and the calculated concentration of 3.47 μmol/s·L ($c(Amylase)_{millifluidic}$ = 0.0347 μmol/s·L). Sample #28 has a dilution factor of 2.5 × 10^3 and the calculated concentration of 122.76 μmol/s·L ($c(Amylase)_{millifluidic}$ = 0.0491 μmol/s·L). The concentration of the patient samples is proportional to the dilution factor and the amylase concentration correlated to the fluorescence intensity detected by the droplet-based millifluidic device. All sample results of PMT fluorescence intensity, dilution factors, and $c(Amylase)_{millifluidic}$ are listed in **Supplementary Table 4**.

Simulation of continuous monitoring patient α-amylase concentration: A pre-set variation of the α-amylase concentration was created by adjusting the injection flow rate ratio between the sample solution (pre-diluted Sample #26 with a dilution factor of 2400) and the reaction buffer while generating droplets. In the droplet sequence, sample dilution fluctuations were generated by tuning the flow rate between the sample and reaction buffer, *e.g.*, dilution 0 (sample vs. buffer = 0:2.5 mL/h) and dilution 1 (sample vs. buffer = 2.5:0 mL/h).

Calculation of LoDs

The calculation of the LoDs is based on the calibration curves and the equations below:

$$LoB = mean_{blank} + 1.645 \times \sigma_b \quad equation(2)$$

$$LoD = LoB + 1.645 \times \sigma_{lc} \quad equation(3)$$

Here, the limit of blank (LoB) is related to the mean signal of blank samples (α-amylase with reaction buffer) and the standard deviation of the blank signal (σ_b). The limit of detection is determined by the limit of blank and the standard deviation of the lowest concentration of samples (σ_{lc}).

Bland-Altman agreement analysis

The Bland-Altman agreement analysis was used to evaluate millifluidic and microplate methods with respect to the clinical method. The analysis was performed by plotting the measured data in specific coordinates. Namely, x-axis shows the mean value measured by two methods and Y-axis is the difference between the measured values of the two methods (*d*).

$$Sample_n(x,y) = (\frac{Clinic_n + Method_n}{2}, Clinic_n - Method_n)$$

To compare differences between the two groups of samples independently of their mean values, the coordinates are chosen as follows: x-axis is the mean value measured by two methods and y-axis shows the ratio of the difference between the measured values of the two methods to the mean value [*d* (Clinic - Method)/mean]. In this case, the y-axis is typically shown in percent:

$$Sample_n(x,y) = (\frac{Clinic_n + Method_n}{2}, \frac{Clinic_n - Method_n}{(Clinic_n + Method_n)/2})$$

n = 1, 2, 3, …., 32, is the sample number. $Method_n$ represents the value of sample n measured by either the droplet-based millifluidic method or the microplate method. $Clinic_n$ means the value of sample n measured by the standard clinical method.

REFERENCES

1. MCACS: How many surgical procedures will Americans experience in an average lifetime?: Evidence from three states. https://mcacs.org/abstracts/2008/P15.cgi.
2. Dobson, G. P. Trauma of major surgery: A global problem that is not going away. *Int. J. Surg.* **81**, 47–54 (2020).
3. Petit, C., Bezemer, R. & Atallah, L. A review of recent advances in data analytics for post-operative patient deterioration detection. *J. Clin. Monit. Comput.* **32**, 391–402 (2018).
4. Knight, S. R. *et al.* Mobile devices and wearable technology for measuring patient outcomes after surgery: a systematic review. *Npj Digit. Med.* **4**, 1–14 (2021).
5. Imani, S. *et al.* A wearable chemical–electrophysiological hybrid biosensing system for real-time health and fitness monitoring. *Nat. Commun.* **7**, 11650 (2016).
6. Ballard, Z. S. *et al.* Computational Sensing Using Low-Cost and Mobile Plasmonic Readers Designed by Machine Learning. *ACS Nano* **11**, 2266–2274 (2017).
7. Nunoo-Mensah, J. W., Rosen, M., Chan, L. S., Wasserberg, N. & Beart, R. W. Prevalence of intra-abdominal surgery: what is an individual's lifetime risk? *South. Med. J.* **102**, 25–29 (2009).
8. Smittenaar, C. R., Petersen, K. A., Stewart, K. & Moitt, N. Cancer incidence and mortality projections in the UK until 2035. *Br. J. Cancer* **115**, 1147–1155 (2016).
9. Nahm, C. B. *et al.* Increased postoperative pancreatic fistula rate after distal pancreatectomy compared with pancreatoduodenectomy is attributable to a difference in acinar scores. *J. Hepato-Biliary-Pancreat. Sci.* **28**, 533–541 (2021).
10. Chikhladze, S. *et al.* The rate of postoperative pancreatic fistula after distal pancreatectomy is independent of the pancreatic stump closure technique - A retrospective analysis of 284 cases. *Asian J. Surg.* **43**, 227–233 (2020).
11. Hank, T. *et al.* Association Between Pancreatic Fistula and Long-term Survival in the Era of Neoadjuvant Chemotherapy. *JAMA Surg.* **154**, 943–951 (2019).

12. Merkow, R. P. *et al.* Postoperative complications reduce adjuvant chemotherapy use in resectable pancreatic cancer. *Ann. Surg.* **260**, 372–377 (2014).
13. Wu, W. *et al.* The impact of postoperative complications on the administration of adjuvant therapy following pancreaticoduodenectomy for adenocarcinoma. *Ann. Surg. Oncol.* **21**, 2873–2881 (2014).
14. Hempel, S. *et al.* Outpatient Drainmanagement of patients with clinically relevant Postoperative Pancreatic Fistula (POPF). *Langenbecks Arch. Surg.* **402**, 821–829 (2017).
15. Müssle, B. *et al.* Drain Amylase or Lipase for the Detection of POPF-Adding Evidence to an Ongoing Discussion. *J. Clin. Med.* **9**, 7 (2019).
16. Davidson, T. B., Yaghoobi, M., Davidson, B. R. & Gurusamy, K. S. Amylase in drain fluid for the diagnosis of pancreatic leak in post-pancreatic resection. *Cochrane Database Syst. Rev.* **2017**, CD012009 (2017).
17. Huggins, C. & Russell, P. S. Colorimetric Determination of Amylase. *Ann. Surg.* **128**, 668–678 (1948).
18. Sjostrom, S. L. *et al.* High-throughput screening for industrial enzyme production hosts by droplet microfluidics. *Lab. Chip* **14**, 806–813 (2014).
19. Holmes, R. J. *et al.* Toward a Microfluidic-Based Rapid Amylase Assay System. *J. Food Sci.* **74**, N37–N43 (2009).
20. L. Cromartie, R., Wardlow, A., Duncan, G. & R. McCord, B. Development of a microfluidic device (μPADs) for forensic serological analysis. *Anal. Methods* **11**, 587–595 (2019).
21. Ultrahigh-throughput screening of industrial enzyme-producing strains by droplet-based microfluidic system | Journal of Industrial Microbiology and Biotechnology | Oxford Academic. https://academic.oup.com/jimb/article/49/3/kuac007/6544676?login=true.
22. Huang, M. *et al.* Microfluidic screening and whole-genome sequencing identifies mutations associated with improved protein secretion by yeast. *Proc. Natl. Acad. Sci.* **112**, E4689–E4696 (2015).

23. Mandal, N., Bhattacharjee, M., Chattopadhyay, A. & Bandyopadhyay, D. Point-of-care-testing of α-amylase activity in human blood serum. *Biosens. Bioelectron.* **124–125**, 75–81 (2019).
24. Dutta, S., Mandal, N. & Bandyopadhyay, D. Paper-based α-amylase detector for point-of-care diagnostics. *Biosens. Bioelectron.* **78**, 447–453 (2016).
25. Pasquardini, L. *et al.* A Surface Plasmon Resonance Plastic Optical Fiber Biosensor for the Detection of Pancreatic Amylase in Surgically-Placed Drain Effluent. *Sensors* **21**, 3443 (2021).
26. Niu, X., Gielen, F., Edel, J. B. & deMello, A. J. A microdroplet dilutor for high-throughput screening. *Nat. Chem.* **3**, 437–442 (2011).
27. Kaminski, T. S. & Garstecki, P. Controlled droplet microfluidic systems for multistep chemical and biological assays. *Chem. Soc. Rev.* **46**, 6210–6226 (2017).
28. Bounab, Y. *et al.* Dynamic single-cell phenotyping of immune cells using the microfluidic platform DropMap. *Nat. Protoc.* **15**, 2920–2955 (2020).
29. Chen, L. *et al.* Millifluidics, microfluidics, and nanofluidics: manipulating fluids at varying length scales. *Mater. Today Nano* **16**, 100136 (2021).
30. Amirifar, L. *et al.* Droplet-based microfluidics in biomedical applications. *Biofabrication* **14**, (2022).
31. Ibarlucea, B. *et al. Real-Time Tracking of Individual Droplets in Multiphase Microfluidics*. (IntechOpen, 2022). doi:10.5772/intechopen.106796.
32. Baraban, L. *et al.* Millifluidic droplet analyser for microbiology. *Lab. Chip* **11**, 4057–4062 (2011).
33. Illing, R. *et al.* Ecotoxicity assessment using ciliate cells in millifluidic droplets. *Biomicrofluidics* **10**, 024115 (2016).
34. Zhao, X. *et al.* Coexistence of fluorescent Escherichia coli strains in millifluidic droplet reactors. *Lab. Chip* **21**, 1492–1502 (2021).
35. Klein, A. M. *et al.* Droplet Barcoding for Single-Cell Transcriptomics Applied to Embryonic Stem Cells. *Cell* **161**, 1187–1201 (2015).

36. Cottinet, D. *et al.* Lineage Tracking for Probing Heritable Phenotypes at Single-Cell Resolution. *PLOS ONE* **11**, e0152395 (2016).
37. White, A. K., Heyries, K. A., Doolin, C., VanInsberghe, M. & Hansen, C. L. High-Throughput Microfluidic Single-Cell Digital Polymerase Chain Reaction. *Anal. Chem.* **85**, 7182–7190 (2013).
38. Schütt, J. *et al.* Compact Nanowire Sensors Probe Microdroplets. *Nano Lett.* **16**, 4991–5000 (2016).
39. Ibarlucea, B. *et al.* Nanowire sensors monitor bacterial growth kinetics and response to antibiotics. *Lab. Chip* **17**, 4283–4293 (2017).
40. Holstein, J. M., Gylstorff, C. & Hollfelder, F. Cell-free Directed Evolution of a Protease in Microdroplets at Ultrahigh Throughput. *ACS Synth. Biol.* **10**, 252–257 (2021).
41. Liu, J. *et al.* A microfluidic based biosensor for rapid detection of Salmonella in food products. *PLOS ONE* **14**, e0216873 (2019).
42. He, S., Joseph, N., Feng, S., Jellicoe, M. & Raston, C. L. Application of microfluidic technology in food processing. *Food Funct.* **11**, 5726–5737 (2020).
43. Nightingale, A. M. *et al.* Monitoring biomolecule concentrations in tissue using a wearable droplet microfluidic-based sensor. *Nat. Commun.* **10**, 2741 (2019).
44. Lapizco-Encinas, B. H. & Zhang, Y. V. Microfluidic systems in clinical diagnosis. *ELECTROPHORESIS* **44**, 217–245 (2023).
45. Long, S. & Berkemeier, B. Ultrasensitive detection and quantification of viral nucleic acids with Raindance droplet digital PCR (ddPCR). *Methods San Diego Calif* **201**, 49–64 (2022).
46. Nakajima, K. *et al.* Low serum amylase in association with metabolic syndrome and diabetes: A community-based study. *Cardiovasc. Diabetol.* **10**, 34 (2011).
47. Nakajima, K. Low serum amylase and obesity, diabetes and metabolic syndrome: A novel interpretation. *World J. Diabetes* **7**, 112 (2016).

48. Chase, C. W., Barker, D. E., Russell, W. L. & Burns, R. P. Serum amylase and lipase in the evaluation of acute abdominal pain. *Am. Surg.* **62**, 1028–1033 (1996).
49. Oh, H.-C. *et al.* Low Serum Pancreatic Amylase and Lipase Values Are Simple and Useful Predictors to Diagnose Chronic Pancreatitis. *Gut Liver* **11**, 878–883 (2017).
50. Amylase Serum and Acute Pancreatitis Diagnosis - Labpedia.net. https://labpedia.net/amylase-serum-and-acute-pancreatitis-diagnosis/ (2020).
51. Batra, H., Kumar, A., Saha, T., Misra, P. & Ambade, V. Comparative Study of Serum Amylase and Lipase in Acute Pancreatitis Patients. *Indian J. Clin. Biochem.* **30**, 230–233 (2015).
52. Vissers, R. J., Abu-Laban, R. B. & McHugh, D. F. Amylase and lipase in the emergency department evaluation of acute pancreatitis11Clinical Laboratory in Emergency Medicine is coordinated by Jonathan S. Olshaker, MD, of the University of Maryland Medical Center, Baltimore, Maryland. *J. Emerg. Med.* **17**, 1027–1037 (1999).
53. Bitter, R., Mohiuddin, T. & Nawrocki, M. : *Advanced Programming Techniques, Second Edition*. (CRC Press, 2017). doi:10.1201/9780849333255.
54. Armbruster, D. A. & Pry, T. Limit of blank, limit of detection and limit of quantitation. *Clin. Biochem. Rev.* **29 Suppl 1**, S49-52 (2008).
55. Bassi, C. *et al.* The 2016 update of the International Study Group (ISGPS) definition and grading of postoperative pancreatic fistula: 11 Years After. *Surgery* **161**, 584–591 (2017).
56. Ratner, B. The correlation coefficient: Its values range between +1/−1, or do they? *J. Target. Meas. Anal. Mark.* **17**, 139–142 (2009).
57. Benesty, J., Chen, J., Huang, Y. & Cohen, I. Pearson Correlation Coefficient. in *Noise Reduction in Speech Processing* (eds. Cohen, I., Huang, Y., Chen, J. & Benesty, J.) 1–4 (Springer, 2009). doi:10.1007/978-3-642-00296-0_5.
58. Doğan, N. Ö. Bland-Altman analysis: A paradigm to understand correlation and agreement. *Turk. J. Emerg. Med.* **18**, 139–141 (2018).
59. Giavarina, D. Understanding Bland Altman analysis. *Biochem. Medica* **25**, 141–151 (2015).

60. Lankatillake, C. *et al.* Screening natural product extracts for potential enzyme inhibitors: protocols, and the standardisation of the usage of blanks in α-amylase, α-glucosidase and lipase assays. *Plant Methods* **17**, 3 (2021).

ACKNOWLEDGEMENTS

The authors would like to acknowledge excellent scientific coordination by Dr. Elisabeth Fischermeier and Dr. Grit Krause-Jüttler (University Hospital and Faculty of Medicine Carl Gustav Carus). We would like to thank Dr. Andrea Leuschner, Dr. Željko Janićijević, and Xuan Peng (both HZDR) for their assistance in taking photographs used in the figures.

FINANCIAL SUPPORT

FRK, JW, and LB were supported through project funding within the Else Kröner Fresenius Center for Digital Health (EKFZ), Dresden, Germany. FRK acknowledges support from the Joachim Herz Foundation (Add-On Fellowship for Interdisciplinary Life Science). LB further acknowledges the financial support of Deutsche Forschungsgemeinschaft (DFG) in the projects Nr.BA4986/8−1 , and GRK 2767; Helmholtz Initiative and Networking Fund in the project 'Mhelthera' (project ID: InterLabs-0031). Furthermore, LB acknowledges the financial support of European Research Council (ERC) in the ERC- Consolidator Grant (ImmunoChip, 101045415).

AUTHOR CONTRIBUTIONS

XZ carried out the experiment. FRK contributed to project conceptualization, patient sample collection and preparation. XZ and FRK wrote the manuscript with support from LB, DM, MB, MD and JW. LB conceived the original idea and supervised the project. All authors provided critical feedback and helped shape the research, analysis, and manuscript.

COMPETING INTERESTS

The authors declare no competing interests.

ORCID FOR CORRESPONDING AUTHORS

Corresponding authors of published papers provide their Open Researcher and Contributor Identifier (ORCID) ID:

Larysa Baraban: 000-0003-1010-2791

Fiona R. Kolbinger: 0000-0003-2265-4809

Supplementary Files

This is a list of supplementary files associated with this preprint. Click to download.

- SIZhao.docx